Orbital Engineering of C_3N Monolayer to Design Efficient Synergistic Sites Electrocatalyst for Boosting Alkaline Hydrogen Evolution

Yamei Zeng,‡[a] Xu Zhang,‡[a] Changzhi Ai,[a] Caizhuang Wang,[b] Yipu Liu,[a,*] Shiwei Lin[a,*]

[a] *State Key Laboratory of Marine Resource Utilization in South China Sea, School of Materials Science and Engineering, Hainan University, Haikou 570228 P. R. China*

[b] *Ames Laboratory-U. S. Department of Energy, and Department of Physics and Astronomy, Iowa State University, Ames, IA 50011, USA*

‡ *These authors have contributed equally to this work.*

* *Corresponding author. E-mail address: linsw@hainanu.edu.cn.*

Abstract

Alkaline water electrolyzer (AWE) is one of the promising technologies for hydrogen production at the industrial level. However, energetic inefficiency and low current density impede the development of AWE. Compared with acidic conditions, the Volmer step in alkaline hydrogen evolution reaction (HER) involves extra water dissociation, whose barrier is one of the most vital reasons for the sluggish kinetics of alkaline HER. Herein, choosing C_3N monolayer as an ideal theoretical model, we design several empty orbitals through intentional metal doping, and further construct synergistic sites on the C_3N monolayer to accelerate both water dissociation and hydrogen adsorption for alkaline HER. The as-designed Be-doped and Cr-doped C_3N monolayers exhibit rather low theoretical overpotential of 0.476 eV and 0.216 eV for alkaline HER, respectively, which are even lower than Pt (111) surface. Moreover, by comparing the water dissociation behaviors on metal-doped C_3N monolayer, we find that the empty orbitals with suitable orientation and energy level are useful for promoting the water dissociation process, indicating that we can use orbital engineering strategy to regulate the adsorption strength between adsorbate and surface site. Consequently, it is reasonable to suggest that our orbital engineering strategy would significantly benefit the design of highly efficient alkaline HER electrocatalysts.

Keywords: metal-doped C_3N; bifunctional catalyst; orbital engineering; water dissociation; density functional theory; alkaline hydrogen evolution reaction

Introduction

Replacing fossil fuels with sustainable energy (e.g., solar and wind power) is one of the crucial steps to address the current environmental crisis and energy shortage.[1] Hydrogen is an ideal energy carrier for achieving the conversation and storage of renewable energy, further resolving the intermittent nature of renewable sources. Alkaline water electrolyzer (AWE) is generally regarded as a promising technology for hydrogen production due to its rather simple configuration and low cost.[2] Moreover, it also provides the possibility of exploring cheaper transition metal-based catalysts, which usually cannot survive under acid condition (proton exchange membrane (PEM) water electrolyzer, for instance).[3, 4] AWE is currently the most widely applied device for hydrogen production at the industrial level. However, energetic inefficiency and low current density impede the development of AWE.[5] Due to the fact that the hydrogen evolution reaction (HER) rate under alkaline condition is typically orders of magnitude slower than in acids, how to accelerate the sluggish hydrogen kinetics is a great challenge associated with AWE.[6] Considering the reaction mechanism of alkaline HER, the hydrogen intermediate (H*) is formed through a water dissociation process ($H_2O + e^- \rightarrow H^* + OH^-$, the Volmer step for HER). Accordingly, the extra water dissociation barrier is always concluded as one of the pivotal reasons for the decreased dynamics and reaction rate of alkaline HER. Therefore, both hydrogen adsorption and water dissociation process should be carefully considered to design highly efficient alkaline HER catalytic structures.[7-9]

In order to promote the water dissociation and hydrogen adsorption simultaneously, the Markovic group developed a bifunctional theory, which suggests that using different functional components to promote the water dissociation and hydrogen adsorption process, respectively. [10, 11] More specially, in a representative catalytic system of "$M_{2+\delta}O_\delta(OH)_{2-\delta}$/Pt", $M_{2+\delta}O_\delta(OH)_{2-\delta}$ provides appropriate adsorption sites for water dissociation, and the nearby Pt sites offer high catalytic sites for hydrogen intermediates.[12] The catalytic activity of as-designed Pt/$Ni(OH)_2$ is 8 times higher than the single Pt catalyst for alkaline HER, indicating the effectivity of such theory. [11] According to this bifunctional promotion mechanism, it is important to figure out effective strategies to regulate the interaction between

intermediates and catalytic structure, further constructing synergistic sites to fascinate different steps of the alkaline HER process. [13, 14]

Based on molecular orbital theory, the interaction strength between adsorbate and surface site can be interpreted by the corresponding bonding and antibonding orbital filling degree.[15] Therefore, it is rational to regulate the interaction strength through orbital engineering, and some related works have already been published.[16] Zang et al. created an empty p_z orbital via carbon doping molybdenum disulfide, which displays an overpotential of 45 mV at 10 mA cm^{-2} under alkaline condition for HER.[17] Additionally, Xie et al. showed that nitrogen-dopant endows empty d_{z^2} orbital in Pt-Ni alloy structure, which can enhance the water dissociation kinetics and further deliver a quite low overpotential of 13 mV at 10 mA cm^{-2} for alkaline HER.[13] Both of these results indicate orbital engineering strategy may be an effective method to enhance alkaline HER. However, due to the difficulty of analyzing orbitals, currently few works are based on this point of view. The as-stated works are actually experimental studies, which means the involved DFT models are specific, and the corresponding analysis is also not quite systemic. Therefore, we want to build appropriate theoretical model structures to investigate this topic systematically.

In this work, using density functional theory (DFT) calculations as an efficient tool, we choose the C_3N monolayer as an ideal model structure to design several kinds of empty orbitals and further systematically explore corresponding alkaline HER activities. Our results prove that empty orbitals with suitable orientation and energy level are useful for promoting the water dissociation process. Moreover, by coupling the surrounding C site, synergistic sites for fascinating both water dissociation and hydrogen adsorption can be established to catalyze alkaline HER. The as-designed Be-doped and Cr-doped C_3N exhibit rather low theoretical overpotential of 0.476 eV and 0.216 eV, respectively, which is even lower than the Pt (111) surface. Additionally, we further present the promotion mechanism of water adsorption and water activation. On the one hand, empty orbitals would accept paired electrons of water molecules, forming bonding orbital to accelerate water adsorption. On the other hand, partial electrons of the metal

atom could transfer to the antibonding orbital of water molecules to weaken O-H bonding. Consequently, our results demonstrate that the orbital engineering strategy is an effective strategy for designing highly efficient catalytic structures for alkaline HER.

Computational Details

All the DFT calculations were performed using the Vienna ab initio Simulation Package (VASP). [18] The exchange-correlation energy was modeled by using Perdew–Burke–Ernzerhof (PBE) functional within the generalized gradient approximation (GGA).[19] The projector augmented wave (PAW) method was used to describe electron-ion interactions.[20] The plane-wave cutoff energy was set to 500 eV for all the calculations, and the convergence threshold was set as 10^{-6} eV in energy and 0.01 eV/Å in force, respectively. The 4 × 2 × 1 supercell of C_3N monolayer (48 C atoms and 16 N atoms in total) was built for further doping, and the optimized structure gives a superlattice dimension of a = 13.4 Å and b = 13.7 Å. A vacuum space of 15 Å was inserted in the z-direction to minimize the interaction between periodic images. The k-point sampling of the Brillouin zone was obtained using a 3 × 3 × 1 grid for the repetitive unit by Monkhorst–Pack scheme. For the density of state (DOS) calculations, a finer 5 × 5 × 1 k-points grid was used to get high accuracy. Additionally, the empirical DFT-D2 correction was employed to improve the van der Waals interaction,[21] and the DFT+U method was performed to correct artificial electron self-interaction for *3d* orbitals of transition metals,[22, 23] and the values of U-J were set as 2.72 eV and 2.79 eV for V and Cr, respectively.[1]

The formation energy (E_f) of metal-doped C_3N (M-C_3N, M = Be, V, Cr) and the binding energy (E_b) between the metal atom and C_3N support were utilized to determine the corresponding structure stability. More specifically, E_f is defined as,[24]

$$E_f = E_{M-C_3N} - E_{C_3N} - \sum_i n_i \mu_i \quad (1)$$

where E_{M-C_3N} and E_{C_3N} denote the total energy of M-C_3N and pristine C_3N, respectively. n_i (i = C, Be, V, Cr) indicates the number of atoms that have been added to ($n_i > 0$, doping atoms) or removed from ($n_i < 0$, C atoms) in M-C_3N, and the μ_i represents the chemical potentials of these species in their bulk states.

According to the above definition, a negative value of E_f suggests that it is thermodynamically feasible to introduce M dopant into C_3N support.

The binding energy (E_b) and the cohesive energy (E_{coh}) were given by these equations[25]

$$E_b = E_{M\text{-}C3N} - E_{C3N\text{-}s} - E_{M\text{-}atom} \quad (2)$$

$$E_{coh} = E_{bulk}/n - E_{M\text{-}atom} \quad (3)$$

where E_{C_3N-s}, and E_{M-atom} represent the total energy C_3N support with the vacancy and metal dopant, respectively. In eq (3), E_{bulk} is the total energy of the bulk state of doping metal, and n is the total number of atoms for the corresponding bulk structure. If the absolute value of E_b is larger than that of E_{coh}, then it means that such M-C_3N system exhibits high thermodynamic stability.

To evaluate the theoretical HER performance of a catalyst under alkaline condition, four elementary steps were considered in our work:

$$* + H_2O \rightarrow H_2O* \quad (4)$$

$$H_2O* \rightarrow H* + OH* \quad (5)$$

$$H* + OH* + e^- \rightarrow H* + OH^- \quad (6)$$

$$H* \rightarrow * + 1/2H_2 \quad (7)$$

The eq (4) and the eq (5) are the water adsorption step and water activation step, respectively, followed by the desorption of OH* (eq (6)) and H_2 production (eq (7)). The thermodynamic analysis of as-stated steps was based on the computational standard hydrogen electrode (CHE) model, as developed by the groups of Nörskov and Rossmeisl.[26] Accordingly, the change of Gibbs free energy of each reaction (ΔG_1, ΔG_2, ΔG_3, ΔG_4) can be calculated as follows, [27]

$$\Delta G_1 = G_{H2O*} - G_{H2O(l)} \quad (8)$$

$$\Delta G_2 = G_{H*} + G_{OH*} - G_{H2O*} \quad (9)$$

$$\Delta G_3 = G_{H2O(l)} - G_{OH*} - 1/2G_{H2} + \Delta G_U + \Delta G_{pH} \quad (10)$$

$$\Delta G_4 = 1/2G_{H2} - G_{H*} \quad (11)$$

For the calculation of Gibbs free energies (G), both enthalpy correction and entropy correction are considered, and detailed calculation method of Gibbs free energy is presented in supporting information.

In addition, ΔG_U and ΔG_{pH} are the terms of bias effect and pH correction, respectively, which can be calculated as follows:[1]

$$\Delta G_U = -eU \quad (12)$$

$$\Delta G_{pH} = -kTln[H^+] = kTln10 \times pH \quad (13)$$

where U is the electrode potential relative to standard hydrogen electrode (SHE), and k and T are the Boltzmann constant and temperature, respectively. In our case, the value of U (pH 14) was determined to be 0.828 V versus SHE according to Nernst equation.[26] Consequently, based on the above definition, the negative ΔG value indicates the corresponding reaction can happen spontaneously.

To identify the kinetic barrier of water dissociation, we constructed minimum energy paths (MEPs) using the climbing image nudged elastic band (CI-NEB) method.[28, 29] The adsorptions of water molecule and OH* + H* pairs were taken as initial state (IS) and final state (FS) of water activation reaction, respectively. Each transition state (TS) was determined by vibrational frequency analysis, which is confirmed through the unique negative eigenvalue of the Hessian matrix of the corresponding structure at the TS. Then, the water activation barrier (G_a) can be calculated by eq (14):[2]

$$G_a = G_{TS} - G_{IS} \quad (14)$$

where G_{TS} and G_{IS} represent the free energy of TS and IS, respectively. Theoretically, a small G_a suggests a fast water activation reaction rate during catalytic reaction.

Results and Discussion

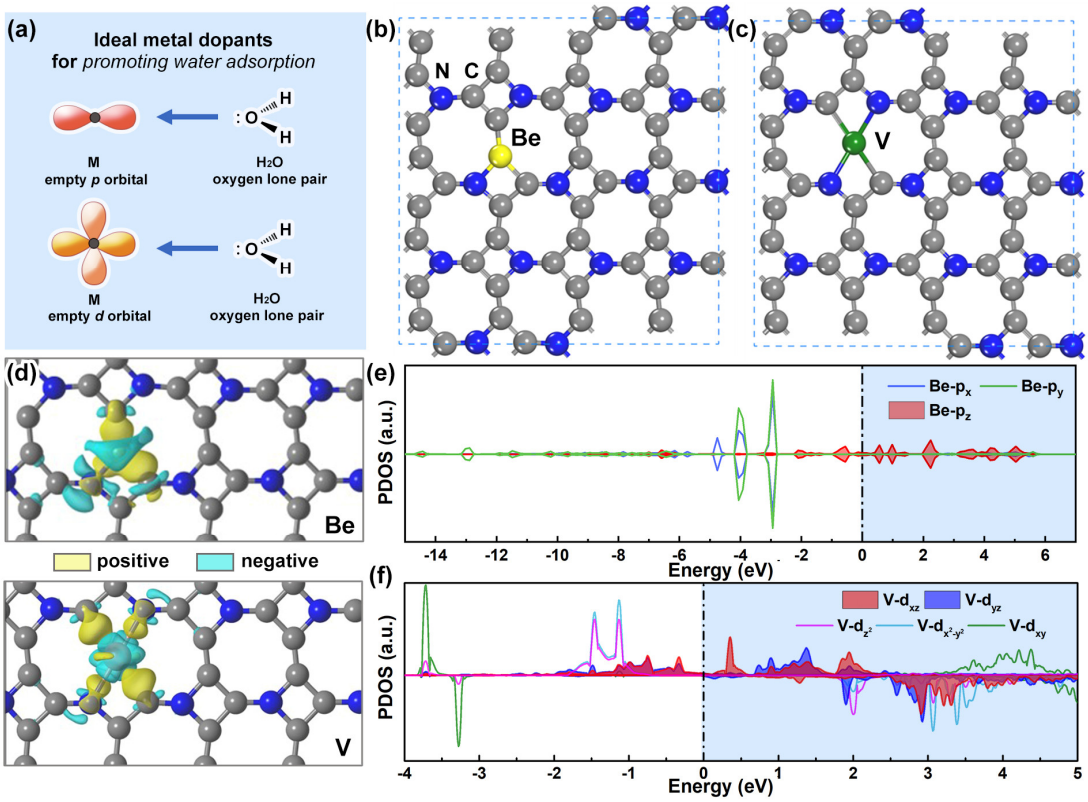

Figure 1. (a) Simplified schematic of H_2O bonding to transition metal dopants with empty orbitals. (b) Top view of the optimized structures of (b) Be-C_3N and (c) V-C_3N monolayers. (d) The charge density difference diagrams of Be-C_3N (upper) and V-C_3N (lower), where the isosurface value is set to be 0.005 e/Å^3. Yellow and blue regions represent electron accumulation and depletion, respectively. The detailed projected density of states for (e) p orbitals of Be ions in Be-C_3N and (f) d orbital of V ions in V-C_3N.

As for alkaline HER, it is generally accepted that the adsorption of water is one of the prerequisites for the whole catalytic reaction,[30] and we try to use an orbital engineering strategy to promote this key process. According to molecular orbital theory, in order to enhance the interaction between two atoms, the orbitals of two atoms need to overlap to form a bonding orbital.[31] Due to the fact that all bonding orbitals of water molecules are occupied, empty orbitals are need to accept the lone-pair electrons of water molecules.[32] Accordingly, we intentionally introduce metal dopants on the surface of catalysts, severing as effective adsorption sites. As shown in Fig. 1a, based on rational orbital orientation, two kinds of orbitals (empty *p* orbital and *d* orbital) are considered in our work. These two orbital orientations can increase the orbital overlapping between catalysts and water molecules, further stabilizing the water

adsorption. Additionally, the new-formed bonding between the adsorption site and water molecule might simultaneously weaken the internal bonding (H-O) in the water molecule, which promotes the as-followed water activation, accelerating the whole water dissociation process.

To achieve our orbital engineering strategy, we choose the C_3N monolayer as the ideal model material, which is derived from the previous high-throughput screening of two-dimensional (2D) metal-free materials for efficient HER.[33] As shown in Fig. S1a in SI, the C_3N monolayer consists of four and eight-membered rings with a planar structure. More specifically, the structure is composed of 3-fold-coordinated C atoms which are bonded to 2 C atoms and 1 N atom, together with 3-fold-coordinated N atoms which are bonded to 3 C atoms. Confirmed by previous work and our results, the C_3N monolayer exhibits metallic behavior with excellent charge transfer performance (Fig. S1b, SI). Moreover, the absolute value of hydrogen adsorption free energy (ΔG_{H*}) on the monolayer C_3N is only 0.14 eV on the C site (Fig. S1c, SI), which is even smaller than that on Pt (111) surface (0.28 eV), demonstrating this structure is one of the potential candidates for catalyzing HER. However, we also found that the C_3N monolayer exhibits sluggish water adsorption and water activation. As presented in Fig. S1d in SI, the Gibbs free energy changes of water adsorption (ΔG_1) and water activation (ΔG_2) are 0.252 eV and 0.5 eV, respectively, implying the C_3N monolayer is not suitable enough for alkaline HER catalysis due to its positive free energies for water adsorption and dissociation. Therefore, we think the C_3N monolayer is an ideal model structure to verify our orbital engineering strategy, and we try to improve the water adsorption by constructing empty orbitals into the structure of the C_3N monolayer.

In order to construct empty *p* and d orbitals on the C_3N monolayer, we first utilized Be and V as suitable dopants. The outer electron configuration of Be atom is $2s^2 2p^0$, and the V atom has a $3d^3 4s^2$ electron arrangement. Due to the difference in atom size, Be dopant prefers to replace a C atom (Be-C_3N), while V atom substitutes a carbon dimer in C_3N (V-C_3N). In the case of the Be-C_3N structure, when the Be atom dopes into C_3N, one electron of Be in the *2s* level would get excited to the *2p* level, further forming sp^2 hybrid orbitals with surrounding 2 C atoms and 1 N atom. Theoretically, one empty *p* orbital

with higher energy than the sp^2 hybrid orbitals can be formed in the Be-C_3N structure. As for V dopants, the V atom would bond with two C atoms and two N atoms in a rectangle-planar geometry, further leading to the energy splitting of five *3d* orbitals of V, and the V dopant would contain empty d orbitals in the V-C_3N structure.[16] Accordingly, the above analysis demonstrates that both Be and V dopant may serve as effective adsorption sites for the water adsorption process, which in accordance with our orbital engineering strategy.

Table 1. The formation energy (E_f), binding energy (E_b) and cohesive energy (E_{coh}) of Be, V, and Cr-doped C_3N monolayers.

	Be-C_3N	**V-C_3N**	**Cr-C_3N**
E_f (eV)	-0.337	-0.783	-1.203
E_b (eV)	-7.30	-8.34	-7.41
E_{coh} (eV)	-3.72	-5.37	-4.02

Based on the above consideration, the optimized structures of Be-C_3N and V-C_3N are further investigated. For Be-C_3N, three possible doping sites were considered, including C1, C2, and N, as shown in Fig. S2a in SI. According to the corresponding defect formation energy (E_f), the Be atom prefers to substitute the C1 atom and fixes on the C_3N surface with an E_f of -0.34 eV (Table S1, SI), and the optimized structure of Be-C_3N is presented in Fig. 1b. Similar to Be-C_3N, there are also three possible doping configurations for V-C_3N (Fig. S2b, SI), and we compared the relevant E_f. Fig. 1c shows the optimized favorable doping structure, where V atom substitutes one carbon dimer of the eight-membered ring and forms two V-C bonds and two V-N bonds with neighboring C and N atoms. By comparing geometric structures before and after Be and V doping monolayer C_3N (Fig. S3, SI), we found that the planar structure is retained, and the length of the C-C and C-N bonds has almost no change. Moreover,

due to the fact that both Be-C_3N and V-C_3N formation energies are negative, we can conclude that both Be and V doping is thermodynamically feasible. We further used the binding energy (E_b) and the cohesive energy (E_{coh}) to evaluate the structural stability of Be-C_3N and V-C_3N. From the E_b and E_{coh} presented in Table 1, the binding energies of Be-C_3N and V-C_3N are -7.30 eV and -8.34 eV, respectively, which are much more negative than the cohesive energy of related metal (-3.72 eV and -5.37 eV), indicating that both Be-C_3N and V-C_3N are relatively stable. The orbital overlap of metals and C, N atoms can also demonstrate the strong interaction among them, as shown in the local density of state of Fig. S4 in SI. All the above results suggest that the chemical interaction between the dopants and the support is strong enough, and both the Be atoms and V atoms can be firmly fixed in the C_3N support.

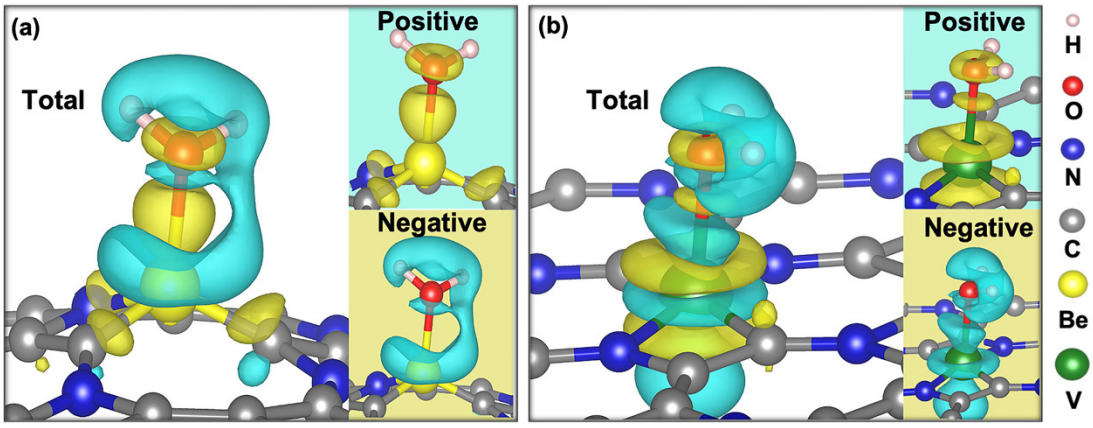

Figure 2. Charge density difference of (a) Be-C_3N and (b) V-C_3N with the adsorption of H_2O molecule, where the isosurface value is set to be 0.002 e/Å^3.

We then investigate the electronic structure of Be-C_3N and V-C_3N. The charge density difference analysis was first investigated to directly demonstrate the charge transfer between the metal center and the C_3N support. As shown in Fig. 1d, electrons transferred from metal atoms to carbon and nitrogen atoms. The difference in charge values of metal atoms and surrounding carbon and nitrogen atoms before and after doping were listed in Table S2, which is obtained for corresponding Bader analysis. More specially, the Be atoms in Be-C_3N and the V atom in V-C_3N transfer 0.482 and 0.252 electrons to adjacent the C2 atom, respectively. Moreover, to confirm the existence of the as-designed empty orbitals in Be-C_3N and V-C_3N, the detailed projected electron density of states (PDOS) for *p* orbitals of Be in Be-C_3N and *d* orbitals of V atom in V-C_3N are further studied. Fig. 1e and Fig. 1f clearly depict that p_z orbital of

Be in Be-C_3N and d_{xz}, d_{yz} orbitals of V in V-C_3N are above Fermi level, indicating that the corresponding orbitals are unoccupied. Therefore, as expected, we successfully introduce empty *p* and *d* orbitals on the monolayer C_3N structure.

We further calculated the free energy of water adsorption (ΔG_{H2O}) for Be-C_3N and V-C_3N to validate our orbital engineering strategy. Additionally, as for control group, the ΔG_{H2O} of B doped C_3N monolayer (B-C_3N, $2s^2 2p^1$), Cr doped C_3N monolayer (Cr-C_3N, $3d^5 4s^1$) and Mn doped C_3N monolayer (Mn-C_3N, $3d^5 4s^2$) also have been calculated. The relevant results together with corresponding E_f, are presented in Table S3 in SI, which are in accord with our assumption. Both Be-C_3N and V-C_3N exhibit a strong interaction with water molecule, the value of ΔG_{H2O} are calculated to be -0.213 eV and -0.444 eV, respectively. As for B dopant, due to the fact that its outer electron configuration ($2s^2 2p^1$) has one more electron compared with Be dopant ($2s^2 2p^0$), therefore we conclude that the doping of Boron might weaken the empty orbit as-generated in Be-C_3N. Accordingly, ΔG_{H2O} of the B-C_3N are calculated to be 0.261 eV, such quite positive value strongly supports our assumption. We further check the PDOS of B-C_3N (Fig. S5), the result also shows that a portion of p_z orbital of B in B-C_3N are below Fermi level, demonstrating that the corresponding orbitals are partially occupied. Besides B-C_3N, both Cr-C_3N and Mn-C_3N also achieve a weak interaction with water molecule (Table S3), confirming the validity of our orbital engineering strategy. In addition, we further check the charge density difference of Be-C_3N and V-C_3N with the adsorption of the H_2O molecules (Fig. 2). The results show that, for both Be and V dopants, the metal atoms not only accept electrons from water molecules but also denote electrons to water. This phenomenon is consistent with our above hypothesis, which is, the empty orbital of metal dopants would accept paired electrons of the water molecule, and simultaneously partial electrons of metal atoms would transfer to the antibonding orbital of water molecules to weaken O-H bonding, further boosting both water adsorption and water activation.

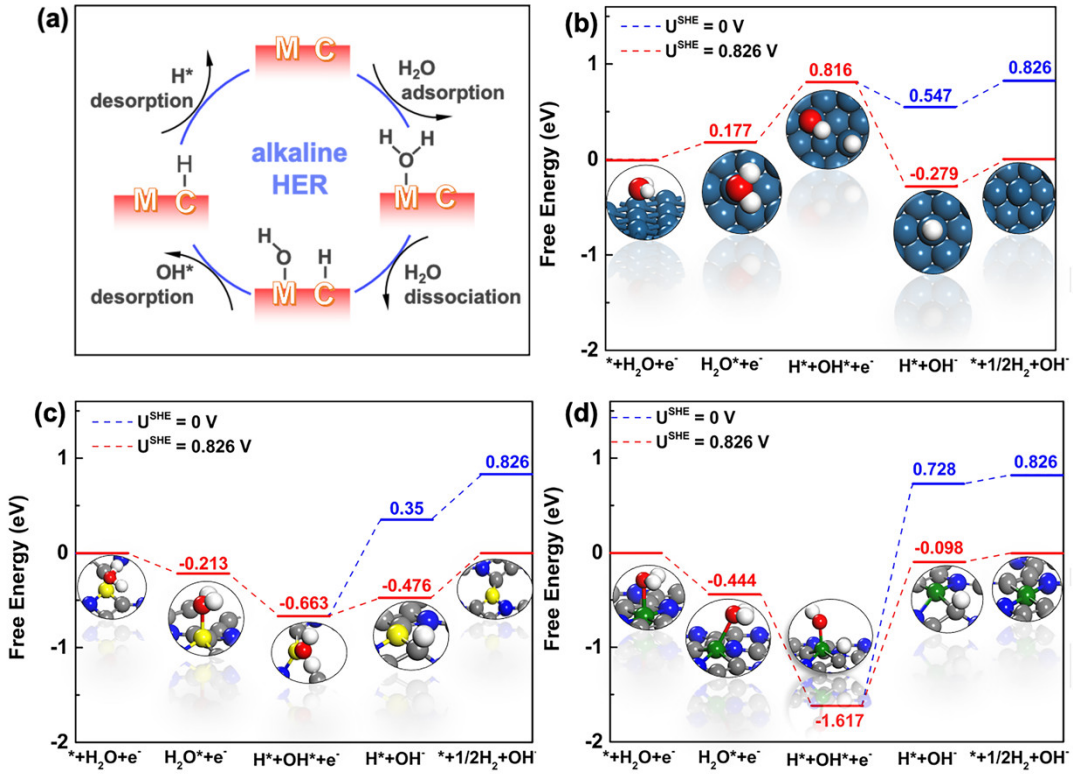

Figure 3. (a) The proposed HER mechanism in alkaline solution, where M and C represent metal dopant as active water dissociation site and carbon sites around the metal, respectively. Free energy diagrams of alkaline HER on (b) Pt (111) surface, (c) Be-C_3N, and (d) V-C_3N monolayer at electrode U = 0 V and U = 0.826 V vs. SHE.

Next, we calculated the free energy diagrams of Be-C_3N and V-C_3N for alkaline HER to determine their catalytic performances. We also applied the Pt (111) surface as a reference due to the fact that it is a widely used theoretical model to represent commercial Pt/C.[1] The involved mechanism for alkaline HER is illustrated in Fig. 3a, and the computed free energy diagrams at an electrode potential of both 0 V and 0.826 V *vs*. SHE are presented. Detailed thermodynamic data used in the free energy of formation calculations and the ΔG values can be found in SI (Table S4 and Table S5 in SI). We first investigate the catalytic behavior of Pt (111). As shown in Fig. 3b, the theoretical overpotential of Pt is 0.64 eV, and the rate-determining step of alkaline HER for Pt is water dissociation, which is consistent with previous reports.[34] As for C_3N based model, we take metal dopant and surrounding carbon atom as water adsorption site and hydrogen adsorption site, respectively, for constructing synergistic sites. For Be-C_3N, Fig. 3c shows that both water adsorption and dissociation are thermodynamic declines, and the corresponding ΔG values are -0.21 eV and -0.45 eV, respectively. Accordingly, the determining step of

Be-C_3N moves to the hydrogen desorption step, and the theoretical overpotential (0.476 eV) is even lower than Pt (111), indicating that the synergistic sites in Be-C_3N exhibit intrinsic catalytic activity for alkaline HER. However, V-C_3N, on the contrary, exhibits a quite large theoretical overpotential of 1.519 eV. As shown in Fig. 3d, the ΔG values of water adsorption and dissociation are -0.44 eV and -1.17 eV, respectively, demonstrating the adsorption and dissociation of water are also automatic. However, the determining step of V-C_3N moves to the hydroxyl desorption step, which indicates that the adsorption of hydroxyl on the V site was too strong to desorb, leading to poisoning of the active site. Therefore, we should further regulate the interaction between intermediates and metal dopants to facilitate the whole alkaline HER.

We further found the Cr atom as another potential dopant based on the *d*-band center theory (Fig. S6, SI) and above results. According to *d*-band center theory, the lower the *d*-band center position of catalytic surface sites, the more electrons would be filled in the as-formed antibonding orbital ((*d*-*σ*)*), leading to a weaker interaction between catalyst and adsorbates.[15] Therefore, it is possible for us to regulate the adsorption strength between the surface structure and the adsorbates through intentionally adjusting the *d*-band center of metal dopants.[35, 36] As shown in Fig. 4a, the *d*-band center of Cr-C_3N is 0.22 eV lower than 0.71 eV of V-C_3N. The whole *d* band of Cr-C_3N moves away from the Fermi level compared with V-C_3N. As expected, the desorption free energy of hydroxyl changed from 2.345 eV to 0.907 eV (Fig. 4b). Together with the crystal orbital Hamilton population (COHP) analysis of V-C_3N and Cr-C_3N (Fig. S7, SI), the filling of the antibonding O-metal *d* states of Cr-C_3N also increases compared with V-C_3N, demonstrating that the interaction between OH and Cr-C_3N is weaker than that of V-C_3N. Additionally, it also should be noted that, when doped into monolayer C_3N, Cr dopant would exhibit an electron configuration of $3d^4$ containing one empty *d* orbital. However, the empty orbital should be ascribed to the d_{xy} according to the corresponding detailed PDOS (Fig. S8, SI). Due to the fact that both the orbital orientation and energy level of d_{xy} in Cr-C_3N cannot match that of H_2O, the determining step of alkaline HER on Cr-C_3N becomes the water adsorption step with an overpotential of 0.216 eV. Finally,

we summarize the adsorption free energy (ΔG_{ads}) of all the four intermedia adsorbates on Pt (111), pure-C_3N, Be-C_3N, V-C_3N, and Cr-C_3N surface at the electrode potential of 0.826 V vs. SHE (Fig. 4c). The absolute ΔG_{ads} values for both Be-C_3N and Cr-C_3N are smaller than Pt (111) and pure C_3N, implying a lower theoretical overpotential of alkaline HER on both Be-C_3N and Cr-C_3N monolayer. Therefore, it can be concluded that from the perspective of thermodynamics, Be-C_3N and Cr-C_3N are promising candidates for alkaline HER owing to the low enough overpotential of 0.476 eV and 0.216 eV, respectively.

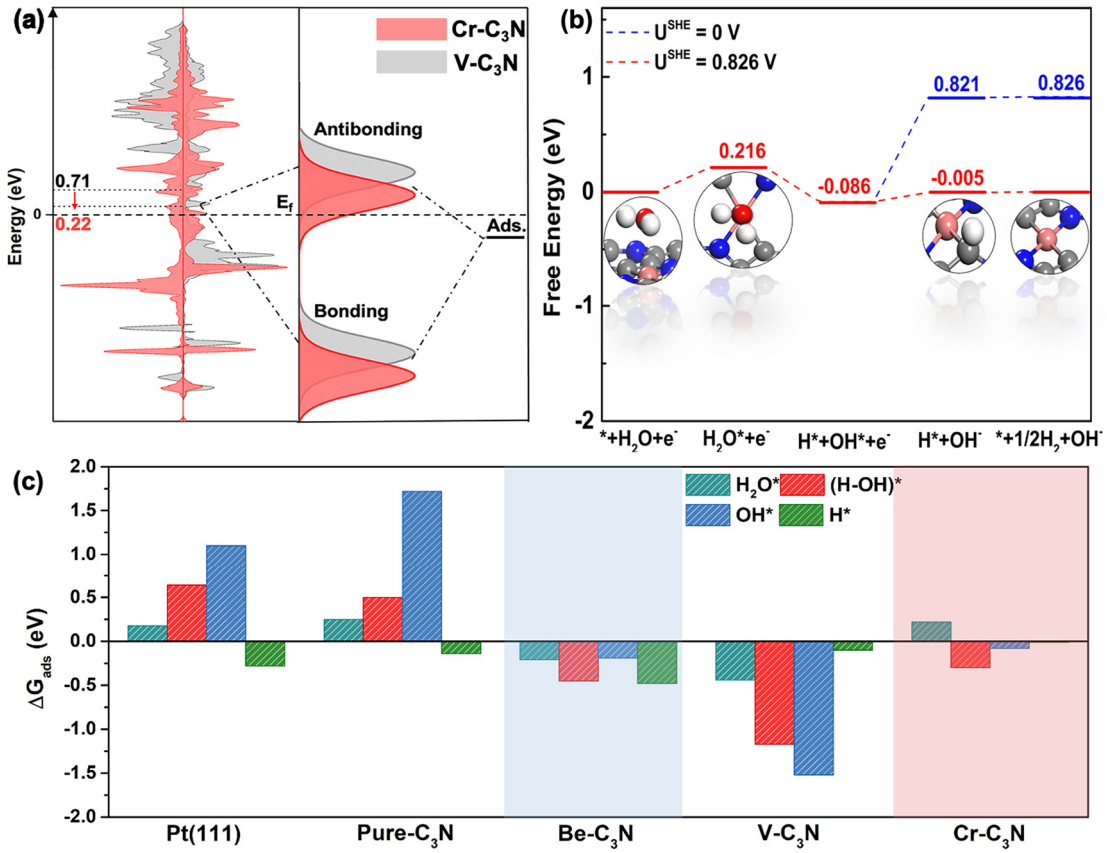

Figure 4. (a) The density of states (DOS) diagrams of d orbitals of V-C_3N and Cr-C_3N as well as the corresponding schematic of bond formation between the catalyst surface and the adsorbate (Ads.). The d-band center positions are marked in the DOS curves. (b) Free energy diagrams of alkaline HER on Cr-C_3N monolayer at electrode U = 0 V and U = 0.826 V vs. SHE. (c) Adsorption free energy (ΔG_{ads}) of hydrogen (H), hydroxyl (OH), water molecule (H_2O), and dissociated water molecule (H-OH) on Pt (111), pure-C_3N, Be- C_3N, and Cr-C_3N surface at electrode U = 0.826 V vs. SHE.

Apart from thermodynamic consideration, we further check the water activation barrier (E_a) of all involved models to investigate the water dissociation process in kinetics aspects. The climbing image nudged elastic band method is used to find the transition state (TS) of water decomposition into OH and

H, where the optimized adsorption models of molecular water and dissociative water are taken as the initial state (IS) and final state (FS), respectively. The corresponding optimized structure for water molecule dissociation on Pt (111) surface, Be-C_3N, V-C_3N, and Cr-C_3N monolayer are presented in Fig. 5. The results show that the O-H bonds in TS exhibit varying degrees of elongation and rotation. By comparing the O-H bond length between TS and IS, it can be concluded that the O-H distances are stretched up to 67% at most for Pt (111), owning the biggest water activation barrier. While the O-H bond of the transition state of water adsorbed on V-C_3N has almost no change showing the lowest barrier. According to the calculation result, the water activation barrier on the Pt (111) surface is 1.12 eV. Meanwhile, the activation barrier of water on these three M-C_3N (M = Be, V, Cr) are lower than Pt, where is 0.54 eV, 0.15 eV, and 0.99 eV, respectively, which is consistent with thermodynamic results mentioned before. Comparing with previous reported results, these water activation barriers are lower than that of many other catalysts, such as C-MoS_2[17], F-Ni_3S_4[14], Co-NiS_2[37], Ru-Ni_5P_4[38], and Se-CoP[6], which behave excellent alkaline hydrogen evolution reaction performance. The detailed comparative data between M-C_3N and previous reported experiment results are shown in Table S6 in SI. In addition, the water dissociative reaction energies (ΔE_{diss}) of all involved models were further analyzed, as presented in Table S7 in SI. The results show that there is a linear trend between Ea and ΔE_{diss}, which is in accord with Bronsted-Evans-Polanyi (BEP) correlation,[39] suggesting that stable adsorption of dissociative water structure (H* + OH*) would lead to a low barrier of water activation. Moreover, the values of ΔE_{diss} for all three M-C_3N are more negative compared with corresponding water adsorption energy, indicating that the H_2O molecule prefers to dissociate rather than desorb on M-C_3N monolayers.

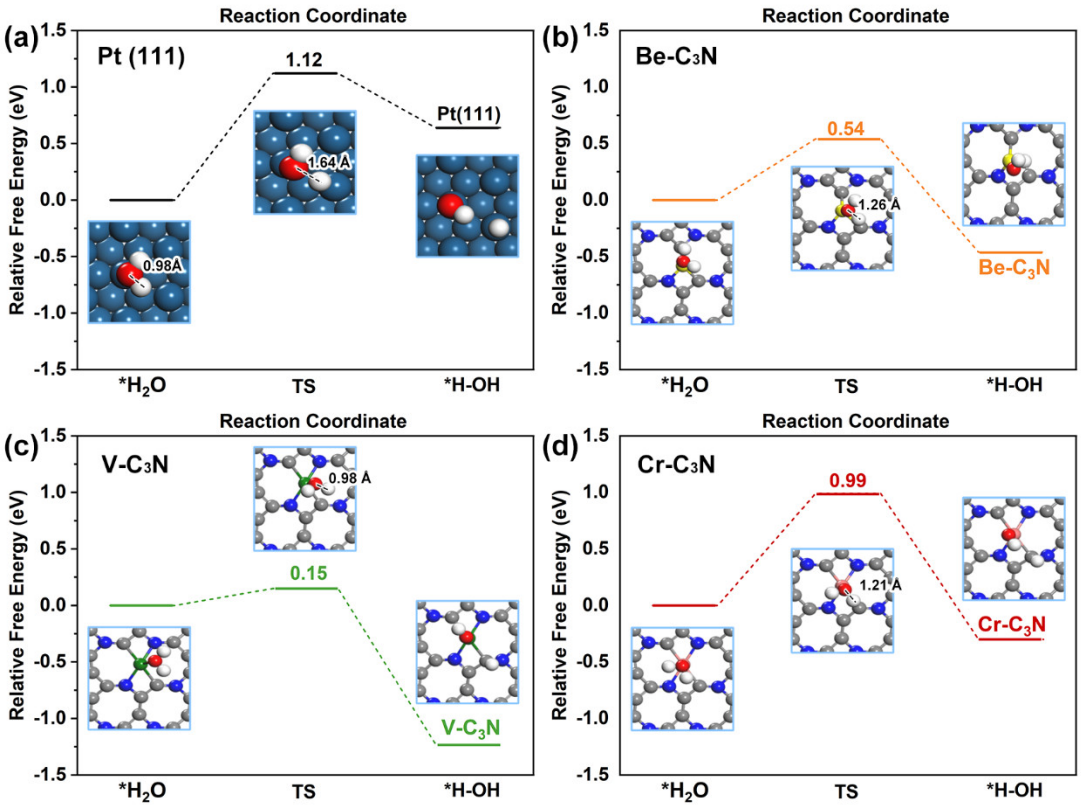

Figure 5. The water dissociation barriers on (a) Pt (111) surface, (b) Be-C_3N, (c) V-C_3N, and (d) Cr-C_3N monolayers. Insets show optimized structures of initial (IS), transition (TS), and final states (FS) of water molecule dissociation. The black dash lines and numbers mark out the O-H bonds and corresponding length.

We then investigate the corresponding electronic structures of involved models to figure out the water dissociation promotion mechanism of metal dopants. Actually, there are two different situations in our work due to different interaction strengths between water and metal dopants, and we will discuss them separately. For Be-C_3N and V-C_3N, the metal dopants have suitable empty orbitals (p_z orbital of Be in Be-C_3N and d_{xz}, d_{yz} orbitals of V in V-C_3N), which can promote the water adsorption effectively. As stated before, we proposed that partial electrons of metal dopant may transfer to the antibonding orbital of water molecules to weaken O-H bonding, further fascinating the water activation step. From the COHP analysis of O-H bonding interaction in H_2O (Fig. 6a), the bonding orbitals of O and H are mainly contributed by p_x and p_z orbitals of O, and all the bonding orbitals of the O-H bond are occupied. [40] Therefore, once p_x or p_z orbital of the O atom bonds with metal dopants, the electrons from the metal atom may transfer directly to the antibonding orbital of the O-H bond, weakening the

corresponding bond strength. We further check the PDOS of Be atoms and V atoms, together with the oxygen atom in H_2O, as presented in Fig. 6b and Fig. 6c, respectively. Results show that O atom contacts with Be atom through p_z orbital (Fig. 6b), and contacts with V atom through p_z and p_x orbital (Fig. 6c). Accordingly, the V atom exhibits strong hybridization with the O atom, giving the lower water activation barrier of 0.15 eV, strongly supporting our as-stated assumption. While in the case of Cr-C_3N, although the mismatched orbital orientation and energy level of the Cr atom lead to rather weak water adsorption, the dissociative water structure on the Cr-C_3N monolayer is quite stable. As shown in Fig. S9 in SI, when OH adsorbed on Cr-C_3N, great orbital overlap can be observed in corresponding PDOS, demonstrating a rather tight interaction, which is the reason why water molecule tends to automatically dissociate into OH and H on Cr-C_3N.

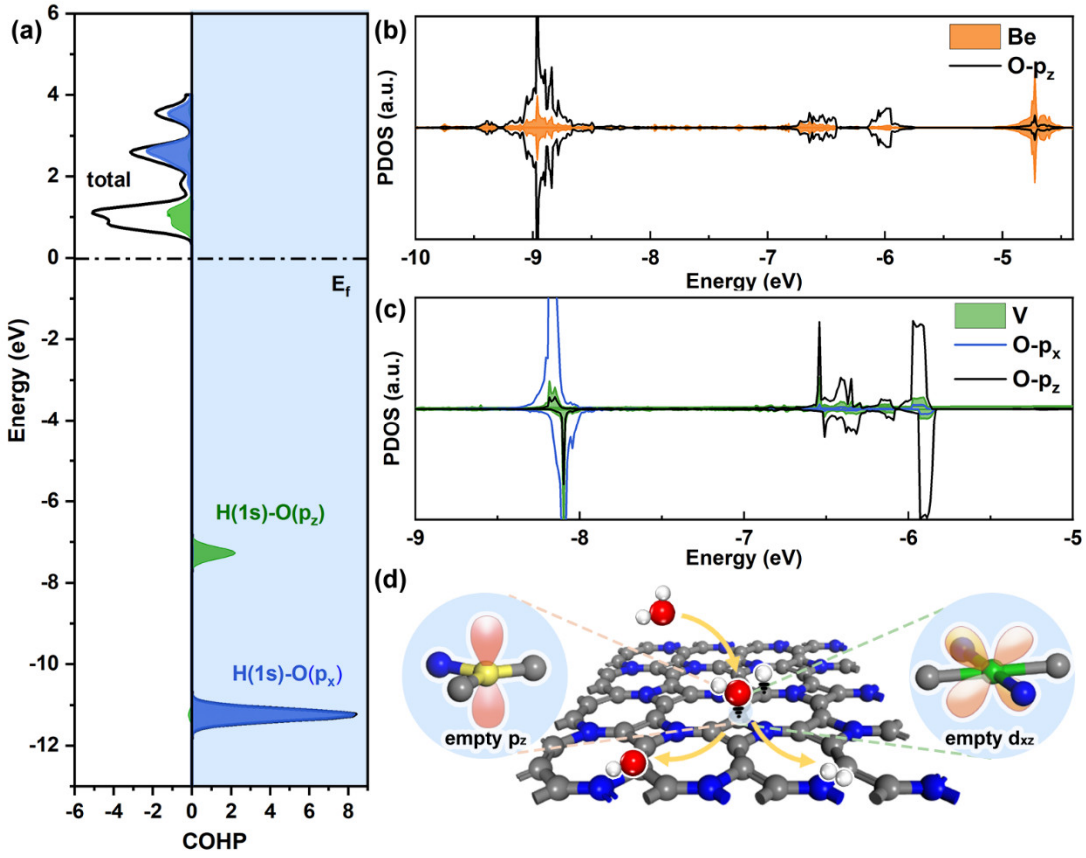

Figure 6. (a) The crystal orbital Hamilton population analysis of O-H bonding interaction in H_2O molecule. The projected electron density of state for (b) Be in Be-C_3N and (c) V in V-C_3N and p_x, p_z orbitals of O atom in H_2O molecule. (d) The mechanism diagram of water molecule dissociation on M-C_3N monolayer and the formation of empty p_z and d_{xz} orbitals via metal doping.

Conclusions

To conclude, in our work, we consider the involvement of the water dissociation process for alkaline HER, further achieving efficient water adsorption and water activation through designing suitable empty orbital. By introducing Be dopant and V dopant into the C_3N monolayer structure, empty p_z orbital and empty d_{xz} orbital are constructed, respectively, exhibiting suited orbital orientation and energy level for water molecules. The calculation results prove that water molecules have strong interaction with the as-formed p_z and d_{xz} empty orbitals, confirming the effectiveness of our design. Additionally, by checking the total reaction free energy results for alkaline HER, we find the desorption of OH is another key step influencing the reaction overpotential. Accordingly, we regulate the OH adsorption energy via tuning the *d*-band center position and we find that Cr dopant exhibits moderate interaction with OH intermediate. The as-obtained Cr-C_3N and Be-C_3N behave rather low theoretical overpotential of 0.216 eV and 0.476 eV, respectively, exhibiting excellent intrinsic catalytic activities. Consequently, as illustrated in Fig. 6d, we successfully design superior synergistic sites to fascinate both water dissociation and hydrogen adsorption for alkaline HER using DFT calculations, further explaining the corresponding promotion mechanism of water adsorption and activation from the perspective of electronic structure. We believe our orbital engineering strategy can serve as a general strategy for enhancing alkaline HER, further will shed some light on the design of other functional catalytic materials.

Acknowledgements. This work was supported by the National Natural Science Foundation of China (Grant Nos. 61764003 and Grant No. 22005116), Hainan Academician Innovation Platform Funding, and the International Postdoctoral Exchange Fellowship Program (20190054). Work at Ames Laboratory was supported by the US Department of Energy, Basic Energy Sciences, Division of Materials Science and Engineering under Contract No. DEAC02-07CH11358, including a grant of computer time at the National Energy Research Scientific Computing Centre (NERSC) in Berkeley, CA.

Table of Contents graphic

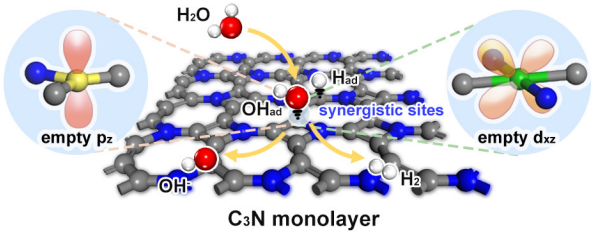

Metal-doped C_3N monolayers with empty orbitals were designed based on orbital engineering strategy for efficient alkaline hydrogen evolution reaction. The as-constructed Be-doped and Cr-doped C_3N monolayer exhibit superior theoretical catalytic activity even better than Pt (111) surface.

References

[1] H. Xu, D. Cheng, D. Cao, X.C. Zeng, A universal principle for a rational design of single-atom electrocatalysts, Nat. Catal., 1 (2018) 339-348.

[2] X. Liu, Y. Jiao, Y. Zheng, K. Davey, S. Qiao, Computational Study on Pt, Ru Dimer Supported on Graphene for Hydrogen Evolution Reaction: New Insight into the Alkaline Mechanism, J. Mater. Chem. A, 7 (2019) 3648-3654.

[3] P. Yu, F. Wang, T.A. Shifa, X. Zhan, X. Lou, F. Xia, J. He, Earth abundant materials beyond transition metal dichalcogenides: a focus on electrocatalyzing hydrogen evolution reaction, Nano Energy, 58 (2019) 244-276.

[4] Z. Chen, X. Duan, W. Wei, S. Wang, B.-J. Ni, Recent advances in transition metal-based electrocatalysts for alkaline hydrogen evolution, J. Mater. Chem. A, 7 (2019) 14971-15005.

[5] M. David, C. Ocampo-Martínez, R. Sánchez-Peña, Advances in alkaline water electrolyzers: A review, J. Energy Storage, 23 (2019) 392-403.

[6] Y. Men, Y. Tan, P. Li, X. Cao, S. Jia, J. Wang, S. Chen, W. Luo, Tailoring the 3d-orbital electron filling degree of metal center to boost alkaline hydrogen evolution electrocatalysis, Appl. Catal., B, 284 (2021) 119718.

[7] Y. Zheng, Y. Jiao, A. Vasileff, S.Z. Qiao, The hydrogen evolution reaction in alkaline solution: from theory, single crystal models, to practical electrocatalysts, Angew. Chem., Int. Ed., 57 (2018) 7568-7579.

[8] T. Kou, M. Chen, F. Wu, T.J. Smart, S. Wang, Y. Wu, Y. Zhang, S. Li, S. Lall, Z. Zhang, Y.-S. Liu, J. Guo, G. Wang, Y. Ping, Y. Li, Carbon doping switching on the hydrogen adsorption activity of NiO for hydrogen evolution reaction, Nat. Commun., 11 (2020) 590.

[9] Y. Liu, Q. Li, R. Si, G.D. Li, W. Li, D.P. Liu, D. Wang, L. Sun, Y. Zhang, X. Zou, Coupling sub-nanometric copper clusters with quasi-amorphous cobalt sulfide yields efficient and robust electrocatalysts for water splitting reaction, Adv. Mater., 29 (2017) 1606200.

[10] X. Wang, Y. Zheng, W. Sheng, Z.J. Xu, M. Jaroniec, S.-Z. Qiao, Strategies for design of electrocatalysts for hydrogen evolution under alkaline conditions, Mater. Today, 36 (2020) 125-138.

[11] R. Subbaraman, D. Tripkovic, D. Strmcnik, K.-C. Chang, M. Uchimura, A.P. Paulikas, V. Stamenkovic, N.M. Markovic, Enhancing hydrogen evolution activity in water splitting by tailoring Li^+-$Ni(OH)_2$-Pt interfaces, Science, 334 (2011) 1256-1260.

[12] R. Subbaraman, D. Tripkovic, K.-C. Chang, D. Strmcnik, A.P. Paulikas, P. Hirunsit, M. Chan, J. Greeley, V. Stamenkovic, N.M. Markovic, Trends in activity for the water electrolyser reactions on 3d M (Ni,Co,Fe,Mn)hydr(oxy) oxide catalysts, Nat. Mater., 11 (2012) 550-557.

[13] Y. Xie, J. Cai, Y. Wu, Y. Zang, X. Zheng, J. Ye, P. Cui, S. Niu, Y. Liu, J. Zhu, Boosting Water Dissociation Kinetics on Pt–Ni Nanowires by N-Induced Orbital Tuning, Adv. Mater., 31 (2019) 1807780.

[14] J. Wang, Z. Zhang, H. Song, B. Zhang, J. Liu, X. Shai, L. Miao, Water Dissociation Kinetic-Oriented Design of Nickel Sulfides via Tailored Dual Sites for Efficient Alkaline Hydrogen Evolution, Adv. Funct. Mater., 31 (2021) 2008578.

[15] B. Hammer, J.K. Norskov, Why gold is the noblest of all the metals, Nature, 376 (1995) 238-240.

[16] Z. Duan, G. Henkelman, Surface Charge and Electrostatic Spin Crossover Effects in CoN_4 Electrocatalysts, ACS Catal., 10 (2020) 12148-12155.

[17] Y. Zang, S. Niu, Y. Wu, X. Zheng, J. Cai, J. Ye, Y. Xie, Y. Liu, J. Zhou, J. Zhu, Tuning orbital orientation endows molybdenum disulfide with exceptional alkaline hydrogen evolution capability, Nat. Commun., 10 (2019) 1-8.

[18] G. Kresse, J. Furthmüller, Efficient iterative schemes for ab initio total-energy calculations using a plane-wave basis set, Phys. Rev. B, 54 (1996) 11169.

[19] J.P. Perdew, K. Burke, M. Ernzerhof, Generalized gradient approximation made simple, Phys. Rev. Lett., 77 (1996) 3865.

[20] G. Kresse, D. Joubert, From ultrasoft pseudopotentials to the projector augmented-wave method, Phys. Rev. B, 59 (1999) 1758.

[21] S. Grimme, Semiempirical GGA-type density functional constructed with a long-range dispersion correction, J. Comput. Chem., 27 (2006) 1787-1799.

[22] S. Dudarev, G. Botton, S. Savrasov, C. Humphreys, A. Sutton, Electron-energy-loss spectra and the structural stability of nickel oxide: An LSDA+U study, Phys. Rev. B, 57 (1998) 1505.

[23] S. Dudarev, G. Botton, S.Y. Savrasov, Z. Szotek, W. Temmerman, A. Sutton, Electronic structure and elastic properties of strongly correlated metal oxides from first principles: LSDA+U, SIC-LSDA and EELS study of UO_2 and NiO, Phys. Status Solidi A, 166 (1998) 429-443.

[24] C.G. Van de Walle, J. Neugebauer, First-principles calculations for defects and impurities: Applications to III-nitrides, Journal of applied physics, 95 (2004) 3851-3879.

[25] M. Yan, Z. Dai, S. Chen, L. Dong, X.L. Zhang, Y. Xu, C. Sun, Single-Iron Supported on Defective Graphene as Efficient Catalysts for Oxygen Reduction Reaction, J. Phys. Chem. C, 124 (2020) 13283-13290.

[26] J.K. Nørskov, J. Rossmeisl, A. Logadottir, L. Lindqvist, J.R. Kitchin, T. Bligaard, H. Jonsson, Origin of the overpotential for oxygen reduction at a fuel-cell cathode, J. Phys. Chem. B, 108 (2004) 17886-17892.

[27] Y. Li, Y. Guo, S. Yang, Q. Li, S. Chen, B. Lu, H. Zou, X. Liu, X. Tong, H. Yang, Mesoporous RhRu Nanosponges with Enhanced Water Dissociation toward Efficient Alkaline Hydrogen Evolution, ACS Appl. Mater. Interfaces, 13 (2021) 5052-5060.

[28] G. Henkelman, B.P. Uberuaga, H. Jónsson, A climbing image nudged elastic band method for finding saddle points and minimum energy paths, J. Chem. Phys., 113 (2000) 9901-9904.

[29] G. Henkelman, H. Jónsson, Improved tangent estimate in the nudged elastic band method for finding minimum energy paths and saddle points, J. Chem. Phys., 113 (2000) 9978-9985.

[30] C.-T. Dinh, A. Jain, F.P.G. de Arquer, P. De Luna, J. Li, N. Wang, X. Zheng, J. Cai, B.Z. Gregory, O. Voznyy, B. Zhang, M. Liu, D. Sinton, E.J. Crumlin, E.H. Sargent, Multi-site electrocatalysts for hydrogen evolution in neutral media by destabilization of water molecules, Nat. Energy, 4 (2019) 107-114.

[31] R. Hoffmann, Solids and surfaces: a chemist's view of bonding in extended structures, John Wiley & Sons, 2021.

[32] M.-A. Légaré, G. Bélanger-Chabot, R.D. Dewhurst, E. Welz, I. Krummenacher, B. Engels, H. Braunschweig, Nitrogen fixation and reduction at boron, Science, 359 (2018) 896-900.

[33] S. Yao, X. Zhang, A. Chen, Z. Zhang, M. Jiao, Z. Zhou, Algorithm screening to accelerate discovery of 2D metal-free electrocatalysts for hydrogen evolution reaction, J. Mater. Chem. A, 7 (2019) 19290-19296.

[34] A.A. Phatak, W.N. Delgass, F.H. Ribeiro, W.F. Schneider, Density functional theory comparison of water dissociation steps on Cu, Au, Ni, Pd, and Pt, J. Phys. Chem. C, 113 (2009) 7269-7276.

[35] F. Lu, D. Yi, S. Liu, F. Zhan, B. Zhou, L. Gu, D. Golberg, X. Wang, J. Yao, Engineering Platinum–Oxygen Dual Catalytic Sites via Charge Transfer towards Highly Efficient Hydrogen Evolution, Angew. Chem, 132 (2020) 17865-17871.

[36] H. Wang, S. Xu, C. Tsai, Y. Li, C. Liu, J. Zhao, Y. Liu, H. Yuan, F. Abild-Pedersen, F.B. Prinz, Direct and continuous strain control of catalysts with tunable battery electrode materials, Science, 354 (2016) 1031-1036.

[37] J. Yin, J. Jin, H. Zhang, M. Lu, Y. Peng, B. Huang, P. Xi, C.H. Yan, Atomic Arrangement in Metal-Doped NiS_2 Boosts the Hydrogen Evolution Reaction in Alkaline Media, Angew. Chem., Int. Ed., 58 (2019) 18676-18682.

[38] Q. He, D. Tian, H. Jiang, D. Cao, S. Wei, D. Liu, P. Song, Y. Lin, L. Song, Achieving efficient alkaline hydrogen evolution reaction over a Ni5P4 catalyst incorporating single-atomic Ru sites, Adv. Mater., 32 (2020) 1906972.

[39] T. Bligaard, J.K. Nørskov, S. Dahl, J. Matthiesen, C.H. Christensen, J. Sehested, The Brønsted–Evans–Polanyi relation and the volcano curve in heterogeneous catalysis, J. Catal., 224 (2004) 206-217.

[40] W.-L. Li, C. Ertural, D. Bogdanovski, J. Li, R. Dronskowski, Chemical Bonding of Crystalline LnB6 (Ln= La–Lu) and Its Relationship with Ln_2B_8 Gas-Phase Complexes, Inorg. Chem., 57 (2018) 12999-13008.